Hot Gas Environment Around STOVL Aircraft in Ground Proximity—Part 2: Numerical Study

D. K. Tafti* and S. P. Vanka†
University of Illinois, Urbana-Champaign, Urbana, Illinois 61801

Ingestion of hot exhaust gases by the engines of Short Take-off and Vertical Landing (STOVL) aircraft has been an important research problem for several years. The hot gas environment around STOVL aircraft is three-dimensional and turbulent. In this study, the Navier-Stokes equations governing the hot gas ingestion flowfield are solved by an efficient finite-difference calculation procedure. The complete geometry, including the head wind and the fuselage, is simulated. Four demonstration calculations with variations in the height of the fuselage and the head wind velocity are presented. It is shown that the calculation procedure efficiently provides a solution to the governing equations, and produces realistic descriptions of the flowfield and temperature field.

Introduction

A NUMBER of interesting fluid dynamic effects have been identified when the lift jets of Short Take-off and Vertical Landing (STOVL) aircraft impinge on the ground surface.[1-3] First, as the lift jets expand, they entrain the surrounding fluid, causing a negative pressure underneath the fuselage and a loss in lift. As the jets impinge on the ground and spread radially outwards, the wall jets further entrain external fluid and increase the loss in lift. In a multiple-jet configuration, these wall jets collide with each other and turn upwards to form an upwash fountain. This fountain flow has two main effects on the STOVL aircraft dynamics. First, an increase in lift force is caused when the fountain impinges on the aircraft fuselage. The recovery in lift is a positive effect of the upwash flow. However, this impinging fluid can also flow along the fuselage surface and eventually make its way into the engine inlets. Because the temperature of the fountain flow is much hotter than the ambient air, its ingestion by the engine can reduce the power and cause thermal stresses in the components. In addition to the fountain flow, another mechanism for hot gas ingestion results from the interaction of the forward-moving wall jet with the headwind. When the headwind and the wall jet collide, a stagnation region is formed, and the wall jet is turned into a ground vortex.[2] This ground vortex can subsequently be re-ingested by the engine, resulting in a further loss in power. However, the hot gas ingestion process depends on where and how the inlets to the engine are located with respect to the approach flow. For strong headwinds, the ground vortex can be pushed behind the engine inlets, such that no hot gases are ingested. It can be recognized that the overall flowfield governing these fluid dynamic interactions is strongly three-dimensional, as well as turbulent.

In the last three decades, a number of studies addressing these issues has been conducted (see Ref. 3 for good review). A majority of these studies were experimental in nature, although some analytical studies of the individual processes, such as single jet impingement, have also been conducted. These studies have identified the fundamental processes and, to a certain extent, quantified the effect of the parameters on hot gas ingestion and fountain flow. However, detailed measurements of the velocity and temperature fields in the fountain region and in the ground vortex in realistic operating conditions are not currently available. Recently, Saripalli[4] conducted some experiments in a water tunnel in which Laser-Doppler velocimeter and laser imaging techniques were used to study the fountain region of the lift jets. These studies involved isothermal flows, and were limited to the fountain formation.

With recent advances in the development of powerful digital computers, it has now become possible to numerically solve the equations that govern the transport of mass, momentum, and enthalpy. However, because the flow is turbulent, such studies must necessarily make assumptions on the macroscopic behavior of turbulence. Despite the inherent limitations of such an approach in representing all the effects of turbulence with precision, it has become a useful engineering tool. Numerical computation of the complete STOVL aircraft flowfield requires the solution of nonlinear partial-differential equations that govern the transport of mass, momentum, and heat in three-dimensional space with boundary conditions that describe the lift jets, aircraft fuselage, and the head wind. Because of the complexity of such solutions and limited computer capabilities, until recently most numerical studies were limited to two dimensions, in which simplifications in the spanwise direction were made. Kotansky and Bower[5] were probably the first investigators to apply a Navier-Stokes analysis to the study of planar jet impingement of relevance to Vertical Take-Off and Landing (VTOL) aircraft. In their analysis, a one-equation model for turbulence kinetic energy was integrated with equations describing the stream function and transport of vorticity. A numerical solution of an impinging jet was obtained and compared with experimental data. This study was followed by Agarwal and Bower,[6] who improved the turbulence model by considering an additional equation for the turbulence dissipation. Because the improved model explicitly calculated the local-length scale of turbulence, the flowfields predicted by their model displayed better agreement with experimental data.

Although the hot gas ingestion process results primarily from the impingement of the lift jets, the eventual ingestion is dictated by the complete flow dynamics, including the formation of the fountain upwash and its interaction with the headwind. For stronger headwind speeds, it is possible to push the ground vortex downstream of the engine inlet and, thus,

Presented as Paper 90-2270 at the AIAA/SAE/ASME/ASEE 26th Joint Propulsion Conference, Orlando, FL, July 16-18, 1990; received Aug. 16, 1990; revision received Dec. 3, 1990; accepted for publication Dec. 27, 1990.

*Research Associate, Department of Mechanical and Industrial Engineering; currently at NCSA-UIUC. Member AIAA.

†Associate Professor, Department of Mechanical and Industrial Engineering. Member AIAA.

completely avoid its contribution to hot gas ingestion. Also, the collision of the wall jets and the fountain formation can be affected by the headwind and the geometry of the fuselage under surface. In addition, placement of Lift Increasing Devices (LIDs)[2] and other obstructions can divert the fountain flow from the engine inlets, thereby reducing the severity of the hot gas ingestion. In order to better understand all the flow processes, a complete Navier-Stokes analysis, including the far-field condition of a prescribed headwind, is necessary. Although such an analysis is computationally very intensive, the benefits are significant for evaluating the effects of geometric and flow parameters. Recently, an important contribution has been made in this direction by VanOverbeke and Holdeman.[7] In this study, the complete fuselage, headwind, and multiple impinging jets were numerically simulated, and the temperature fields close to the engine inlet face were studied. By varying the head wind and the impingement height, they were able to alter the ingestion pattern and quantify their effects. A finite-difference computer program[8] was used, and the flow domain was discretized into a relatively large number of finite volumes.

A primary drawback of numerical computations of three-dimensional elliptic fluid flows is that they can require substantial amounts of computer time to obtain a converged solution. These large computational costs often discourage systematic and thorough investigations of the effects of various parameters. However, with research into faster converging numerical algorithms, it is possible to substantially reduce these computer times. In this paper, we demonstrate the applicability of one such algorithm,[9] which is based on the concept of using multiple levels of grids[10] to obtain faster convergence. In this study, the geometrical configuration studied by VanOverbeke and Holdeman[7] is considered, and a set of four calculations have been performed. To compare our results with those of VanOverbeke and Holdeman,[7] we have simulated exactly the same configurations, albeit with a finer grid, and compared the computer times and the flowfields. The four calculations in this study differ in the height of the jets from the ground and the ratio of the head wind to the jet velocity.

The following sections briefly describe the solution procedure and present the results of the calculations. In Part 1 of this study, a separate experimental investigation is presented by McLean et al.,[11] in which the concentration of the exhaust jets is quantified through a laser imaging technique.

Governing Equations and Solution Algorithm

The flowfield and temperature field around the STOVL aircraft are governed by the following set of elliptic partial-differential equations. In the present analysis, the flow is considered to be steady in the time-averaged sense, and the effects of turbulence are captured by a turbulence model.[12] The governing equations can be written as follows:

$$\text{mass continuity: } \frac{\partial}{\partial x}(\rho u) + \frac{\partial}{\partial y}(\rho v) + \frac{\partial}{\partial z}(\rho w) = \dot{m} \tag{1}$$

$$x\text{-momentum: } \frac{\partial(\rho uu)}{\partial x} + \frac{\partial(\rho uv)}{\partial y} + \frac{\partial(\rho uw)}{\partial z} = -\frac{\partial P}{\partial x} + \frac{\partial}{\partial x}\left(2\mu\frac{\partial u}{\partial x}\right) + \frac{\partial}{\partial y}\left[\mu\left(\frac{\partial u}{\partial y} + \frac{\partial v}{\partial x}\right)\right] + \frac{\partial}{\partial z}\left[\mu\left(\frac{\partial w}{\partial x} + \frac{\partial u}{\partial z}\right)\right] + \dot{m}u_{inj} \tag{2}$$

$$y\text{-momentum: } \frac{\partial(\rho uv)}{\partial x} + \frac{\partial(\rho vv)}{\partial y} + \frac{\partial(\rho vw)}{\partial z} = -\frac{\partial P}{\partial y} + \frac{\partial}{\partial x}\left[\mu\left(\frac{\partial u}{\partial y} + \frac{\partial v}{\partial x}\right)\right] + \frac{\partial}{\partial y}\left(2\mu\frac{\partial v}{\partial y}\right) + \frac{\partial}{\partial z}\left[\mu\left(\frac{\partial w}{\partial y} + \frac{\partial v}{\partial z}\right)\right] + \dot{m}v_{inj} \tag{3}$$

$$z\text{-momentum: } \frac{\partial(\rho uw)}{\partial x} + \frac{\partial(\rho vw)}{\partial y} + \frac{\partial(\rho ww)}{\partial z} = -\frac{\partial P}{\partial z} + \frac{\partial}{\partial x}\left[\mu\left(\frac{\partial w}{\partial x} + \frac{\partial u}{\partial z}\right)\right] + \frac{\partial}{\partial y}\left[\mu\left(\frac{\partial v}{\partial z} + \frac{\partial w}{\partial y}\right)\right] + \frac{\partial}{\partial z}\left(2\mu\frac{\partial w}{\partial z}\right) + \dot{m}w_{inj} \tag{4}$$

$$\text{turbulence energy: } \frac{\partial}{\partial x}(\rho uk) + \frac{\partial}{\partial y}(\rho vk) + \frac{\partial}{\partial z}(\rho wk) = \frac{\partial}{\partial x}\left(\Gamma_k\frac{\partial k}{\partial x}\right) + \frac{\partial}{\partial y}\left(\Gamma_k\frac{\partial k}{\partial y}\right) + \frac{\partial}{\partial z}\left(\Gamma_k\frac{\partial k}{\partial z}\right) + G - \rho\varepsilon + \dot{m}k_{inj} \tag{5}$$

$$\text{dissipation of turbulence energy: } \frac{\partial}{\partial x}(\rho u\varepsilon) + \frac{\partial}{\partial y}(\rho v\varepsilon) + \frac{\partial}{\partial z}(\rho w\varepsilon) = \frac{\partial}{\partial x}\left(\Gamma_\varepsilon\frac{\partial\varepsilon}{\partial x}\right) + \frac{\partial}{\partial y}\left(\Gamma_\varepsilon\frac{\partial\varepsilon}{\partial y}\right) + \frac{\partial}{\partial z}\left(\Gamma_\varepsilon\frac{\partial\varepsilon}{\partial z}\right) + C_1G\frac{\varepsilon}{k} - C_2\rho\frac{\varepsilon^2}{k} + \dot{m}\varepsilon_{inj} \tag{6}$$

$$\text{enthalpy: } \frac{\partial}{\partial x}(\rho uH) + \frac{\partial}{\partial y}(\rho vH) + \frac{\partial}{\partial z}(\rho wH) = \frac{\partial}{\partial x}\left(K\frac{\partial T}{\partial x}\right) + \frac{\partial}{\partial y}\left(K\frac{\partial T}{\partial y}\right) + \frac{\partial}{\partial z}\left(K\frac{\partial T}{\partial z}\right) + \dot{m}H_{inj} \tag{7}$$

$$\text{equation of state: } \rho = P/RT \tag{8}$$

where u, v, w, are the velocities in the x, y, and z directions, respectively; P is the pressure, R is the gas constant, and G is the production of turbulent kinetic energy. In all these equations, the diffusive coefficients contain the effects of laminar as well as turbulent diffusion. Standard values of the constants in the turbulence model[12] are used.

These equations are solved on a rectangular domain that envelopes the aircraft fuselage and the exhaust jets. Because the current computer program is limited to the use of rectangular grids, the fuselage of the aircraft was modeled to be of rectangular shape. However, efforts are currently under way to extend the program to handle grids of arbitrary inclinations (boundary-fitted grids), which will then permit a more realistic representation of the aircraft shape and angles of attack. The boundary conditions and solution domain considered in current calculations will be described in a later section.

The above equations are finite-differenced by a hybrid scheme[9] combining first- and second-order differencing for the total convective and diffusive operator. At high-cell Peclet numbers, the finite-differencing scheme becomes first-order accurate to preserve stability of the solution procedure. The multigrid solution technique[10] differs from the single grid technique in the manner the finite-difference equations are solved to the required accuracy. It is well-known that, for elliptic equations, single grid techniques converge poorly when the

finite-difference grid contains a large number of mesh points. This results from the low-frequency errors that are slow to converge on a given fine grid. In the multigrid concept, a series of fine and coarse grids are used, and the solution is switched between the coarse and fine grids such that errors of all frequencies converge at the same rate. This novel concept was originally proposed for model elliptic equations, but recently it has become popular in solving practical fluid flows.

The principle behind the multigrid procedure may be explained as follows. Consider an elliptic equation that is discretized by finite-difference or finite element methods. Generally, an iterative procedure that is designed to obtain a solution to the discrete equations will converge rapidly in the first few iterations, but subsequently the convergence deteriorates. It can be shown through formal analyses that the cause for this poor convergence is the presence of low-frequency errors that are not resolved well on any given grid. However, these errors can converge faster if the grid is coarse; therefore, in the multigrid procedure, these errors are interpolated to a coarser grid and solved. The results of this coarse grid solution are then put back on the finer grid solution through extrapolation. In the case of a calculation with many mesh points, several layers of coarse meshes can be used to obtain rapid convergence. However, the coarsest grid is often dictated by the constraints of geometry and boundary conditions.

In the present solution scheme, we have combined the multigrid technique with a coupled solution scheme for the momentum and continuity equations. The velocities and pressures are obtained by a block-implicit solution of the momentum and continuity equations. Because this procedure is explained in previous works by one of the authors,[9] it is not elaborated on here. However, in order to simulate the fuselage and the lift jets, the procedure has been extended to handle internal obstacles and mass and momentum injections. These features have been incorporated in a manner that maintains consistency between the coarse and fine grids—a necessary feature for the algorithm to eventually converge to the correct solution. It must be pointed out that, although the coarse grids are used, the final solution is obtained on the finest grid in the system. Thus the intermediate grids are used only for accelerating the convergence rate, and do not influence the final converged solution.

The present computer program was initially validated in model laminar flow problems prior to being used for more complex flows. Recently, the computer program was applied to calculate the interaction of a transverse jet with a cross-stream flow.[13] Also, the program was validated by applying it to studying the twin-jet upwash flow in isolation and comparing[14] the resulting solutions with the experimental data of Saripalli.[4] These two studies, as well as a calculation of a single jet impingement (unpublished), provide confidence in the use of the present computer program to the complete STOVL configuration.

The next section describes the computational domain and a typical convergence history of the multigrid solution procedure. Simulated flowfields and temperature fields are presented, along with a discussion on the mechanism of hot gas ingestion for a four-jet configuration. These results compare qualitatively with the flow imaging data of McLean, Sullivan, and Murthy,[11] as well as with calculations presented by Van Overbeke and Holdeman.[7]

Results

Computational Details and Convergence Histories

In this study, four test cases have been considered, which are similar to those studied in Ref. 7. The important flow and geometrical parameters are outlined in Table 1. The four cases differ in the height of the fuselage from the ground plane (h/d, where d is the diameter of the lift jets) and the headwind to jet velocity ratio (U_∞/U_j). The solution domain is a three-dimensional wind tunnel with overall dimensions of 136d in the streamwise direction (x), 27 or 29d in the cross-stream direction (y), and 40d in the spanwise direction (z). These large dimensions are necessary to accurately resolve the flowfield around the jets and the fuselage without any interference from the simulated boundaries. Figure 1 shows the computational grid used and the flow geometry. The geometry simulates four jets (due to symmetry, only half the domain is considered) issuing from the engine with the engine inlet located 10 jet diameters upstream of the fore jet axis. The distance between the fore and aft jet axis is 6 diameters; the spanwise distance between the jets is 3.2 diameters. The fuselage extends throughout the calculation domain, and is 2.5 diameters in height and 2.2 diameters in width. The inlet, which is 67 jet diameters from the entrance of the test section, has a height of 2.5 diameters and a width of 1.4 diameters. It is adjacent to the fuselage in the spanwise direction and extends 9.5 jet diameters up to the fore jet, after which it becomes part of the fuselage. The calculation domain is divided into 100 computational cells in the x direction, 44 in the y, and 48 in the z direction, giving a total of about 211,000 cells. The particular grid distribution was chosen to provide good resolution in the near field of the jets and, at the same time, keep the grid expansion ratio as small as possible. The grid distribution was also influenced by the necessity to accommodate internal obstacles and baffles, such that grid lines bounded the surfaces of these structures.

At the inlet of the test section, uniform velocity and temperature conditions are prescribed for the incoming headwind; the turbulent kinetic energy was assumed to be 1% of the mean kinetic energy. At the exit, outflow boundary con-

Table 1 Flow and geometry parameters

Case	U_∞/U_j	h/d	Ma_j	$Re_\infty \times 10^{-4}$	$Re_j \times 10^{-5}$
1	0.03	4.0	0.47	3.3	3.3
2	0.03	2.0	0.47	3.3	3.3
3	0.09	4.0	0.47	9.9	3.3
4	0.09	2.0	0.47	9.9	3.3

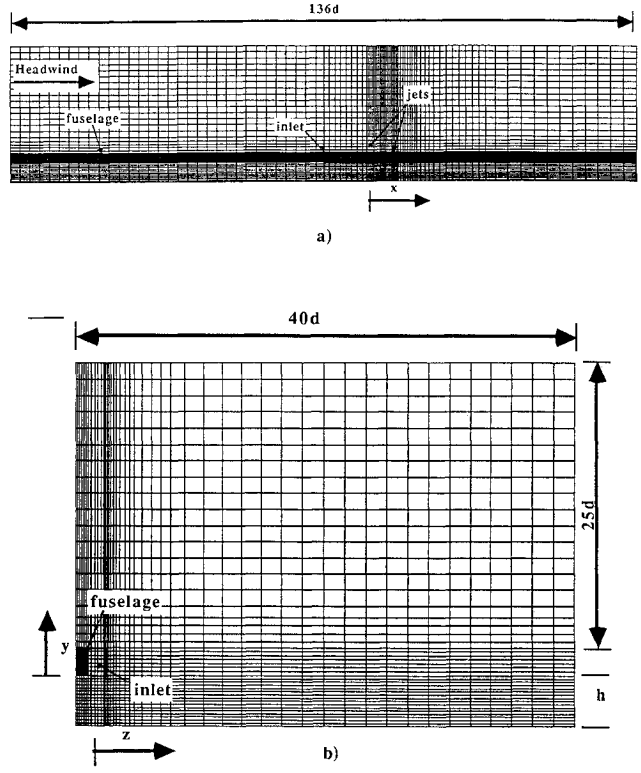

Fig. 1 Computational domain and grid distribution: a) side view; b) front view (not to same scale as a)).

ditions are prescribed. In the y direction, wall boundary conditions are prescribed. The bottom wall is assumed to have zero heat loss, whereas the top wall is assumed to be at a uniform temperature. In the spanwise direction, symmetry boundary conditions are applied on one side, whereas an adiabatic wall is prescribed on the other side. Within the calculation domain, additional conditions are prescribed for the engine inlet and the jets. The inlet acts as a mass sink, the jets as mass sources. In prescribing these conditions, it is important to conserve mass. The jet velocity profile is assumed to be uniform, with the turbulent kinetic energy equal to 1% of the mean kinetic energy.

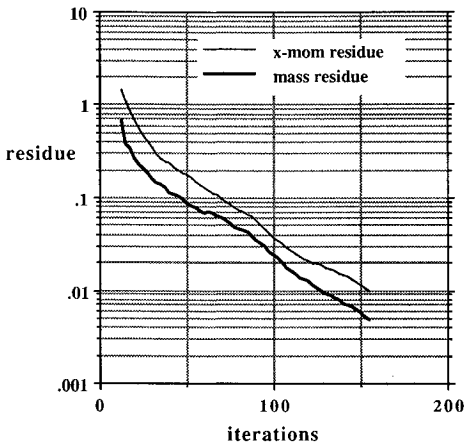

Fig. 2 Typical convergence history for multigrid calculation procedure, 100 × 44 × 48 cells with two coarse levels.

In the calculation procedure, the prescribed fine grid was coarsened to two additional levels. The calculation was started on the coarsest grid from prescribed initial conditions, but, on the finer grids, the starting solutions were obtained by successively extrapolating converged flowfields from the coarser grids. This Full Multigrid Cycle (FMG) provided realistic starting values for the calculations on the fine grids. Figure 2 shows a typical convergence history for the calculation of case 1. The convergence is monitored by the normalized sum of the absolute mass and momentum residuals over the whole solution domain. It is seen that the solution converges to the required tolerance of 1% error in approximately 150 iterations. In the previous study of VanOverbeke and Holdeman,[7] which used a single grid procedure, the number of iterations were approximately 2000 for a 134,000 grid. This represents a significant reduction in computational effort. The present calculation required approximately 35 min of CPU time on a CRAY-2; typically, this translates to a few hours of interactive real clock time.

Calculated Velocity and Temperature Fields

Hot gas ingestion is a serious problem for STOVL aircraft in ground proximity. Two important factors governing hot gas

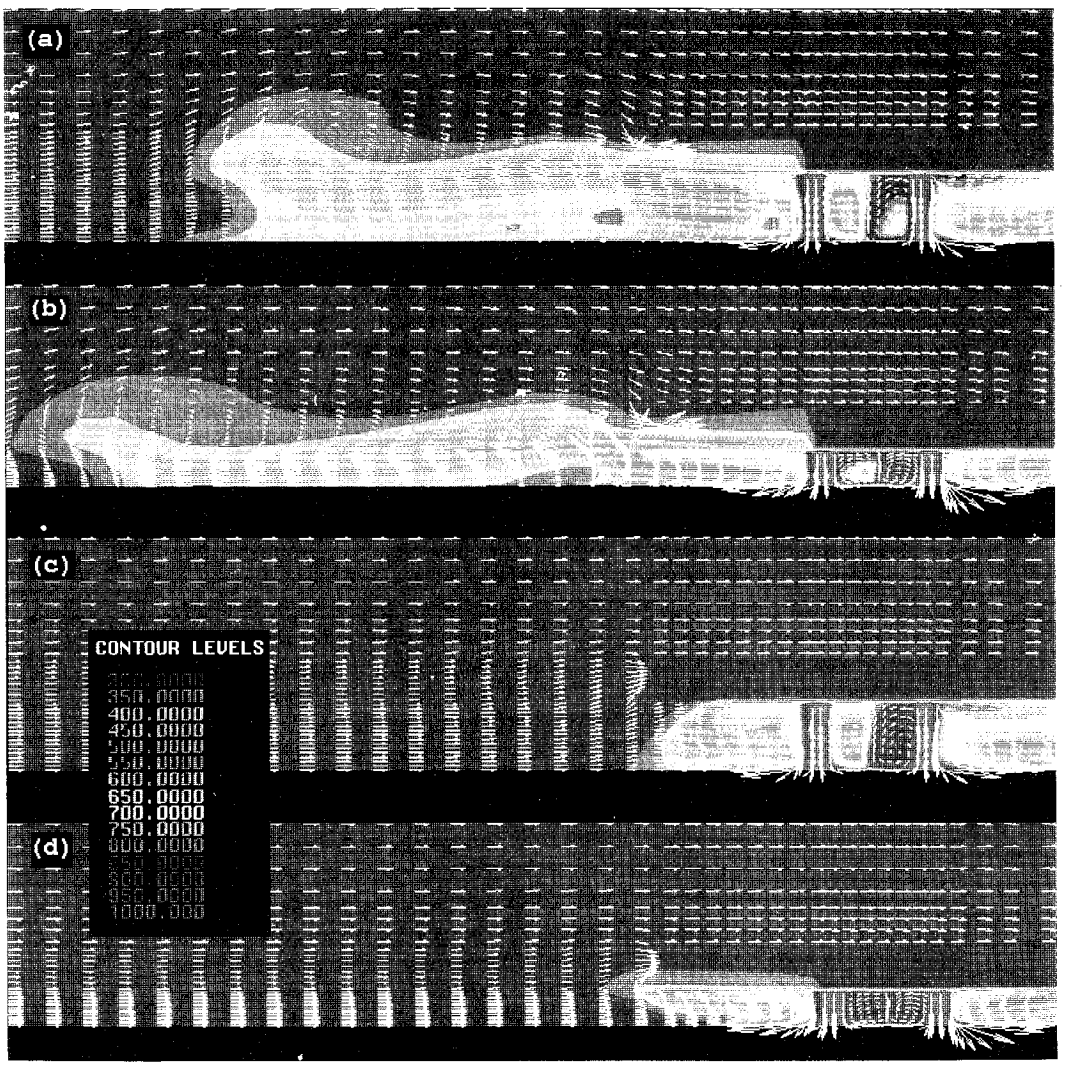

Fig. 3 Superimposed velocity vectors and temperature gray scale contours in x-y plane through the jet centerline (z = 0). Plot domain extends from $-46 \leq x/d \leq 14$ and from the ground plane to y/d = 20: a) case 1; b) case 2; c) case 3; d) case 4; headwind from left to right.

ingestion are the proximity of the lift jets to the ground (h/d ratio) and the ratio of the freestream velocity to the jet velocity (U_∞/U_j). Two other important factors, not considered in the present study are the location of the inlet with respect to the life jets and the use of shields and baffles to deflect the flow of hot gases away from the engine inlet. When the lift jets impinge on the ground, they stagnate and form radially flowing wall jets. When two opposing wall jets meet, they manifest themselves into a fountain flow. The flowfield caused by a rectangular four-jet configuration is governed by a strong fountain flow between the fore and aft jets (streamwise fountain) and also between the symmetrical spanwise jets (spanwise fountain). The streamwise fountain upwash, when obstructed by the fuselage, is forced to flow laterally outwards and up, whereas the spanwise fountain upwash tends to flow under and along the length of the fuselage in the streamwise direction. Both these mechanisms contribute to the direct ingestion of hot gases into the inlet. The other mechanism of hot gas ingestion, which is not as severe, is due to the recirculating flow caused by the interaction of the outward flowing hot gases with the headwind. The outward flowing hot gases are forced to stagnate by the freestream flow, and are deflected towards the engine inlet where they are reingested.

Figure 3 shows velocity vectors superimposed on gray scale temperature contours in the x-y plane passing through the center of the fore and aft jets for the four cases. (For the sake of clarity, different vector scales are used in different segments of the domain.) The effect of headwind to jet velocity ratio (U_∞/U_j) on the flowfield is clearly evident. In cases 1 and 2 ($U_\infty/U_j = 0.03$), the effect of the lift jets extends far upstream (35 jet diameters for case 1 and 46 jet diameters for case 2), whereas for cases 3 and 4 ($U_\infty/U_j = 0.09$), the stagnation region is much closer to the jets. For the low-velocity ratio, hot gas from the lift jets flows under the fuselage towards the inlet, where part of it is ingested directly by the strong suction of the inlet, while the rest is carried by its streamwise momentum further upstream until it is forced to stagnate by the oncoming flow and recirculate back towards the inlet (ground vortex). The most striking difference between high and low U_∞/U_j is the complete absence of the recirculating ground vortex in cases 3 and 4. This is due to the high forward momentum of the headwind, which prevents the hot gas from the jets from moving upstream. The effect of different h/d ratios is not as strong. For h/d of 2 (cases 2 and 4), a smaller area is available between the fuselage and the ground and, consequently, the radial momentum of the hot gas is larger than for h/d of 4. This enhances the spread of the jet, both in the lateral and streamwise direction. A comparison of cases 3 and 4 (just upstream of the fore jet and under the fuselage) suggests that for h/d of 2 the forward flow is stronger than for h/d of 4. This is also the case for cases 1 and 2, in which the recirculating zone for h/d of 2 extends about 11 jet diameters further upstream than for h/d of 4.

In all cases, the temperature fields upstream of the lift jets are very similar to those implied by the velocity field. For cases 1 and 2 ($U_\infty/U_j = 0.03$), the hot gases from the jets are transported much further upstream of the inlet. The upstream transport and the subsequent recirculation of hot gases (although cooler) back to the inlet can be directly correlated with the velocity vector field. In Figs. 3a and 3b, the cooler recirculated gases (positive streamwise velocity) can be clearly distinguished from the hotter gases (negative streamwise velocity). This relation between the velocity field and the temperature field is also evident in case 4 ($U_\infty/U_j = 0.09$, h/d = 2) between the inlet and the fore jet, where hot gases are transported upstream along the bottom of the fuselage. However, for case 3 ($U_\infty/U_j = 0.09$, h/d = 4), the temperature field extends further upstream than indicated by the velocity field. This indicates either a diffusive transport of heat or convective transport of heat from the sides. Another interesting feature is the difference in temperature between the fore half of the fountain and the aft half. In all cases, the fore half is cooler than the aft half, which must be due to its greater interaction with the cooler freestream fluid. This effect was also observed in the simulations in Ref. 7. Maclean et al.[11] compared the upstream distribution of temperature (along the jet center and along the axis of symmetry) obtained from their experiments with the present calculations for case 3. In the region near the jets, the agreement between the two is good, but further upstream the experiments show a higher concentration of jet fluid.

Figure 4 shows gray scale contours of the temperature field in the ground plane. For the low headwind case, there is much more forward and lateral spread of the hot gases than with the higher headwind. In addition, the height of the fuselage above the ground (h/d ratio) also has an effect on the forward and lateral spreading of the jets. As mentioned earlier, for h/d = 2, the radial momentum of the jet is higher, as can be seen in the greater lateral spread of the jet fluid before it is pushed downstream by the headwind. Another interesting feature is the sharp temperature gradients observed between the jets in the fountain upwash region. This is due to the vertical movement of two jet streams at different temperatures, with little transverse movement of fluid across this boundary. In fact, the locus of points across which these sharp gradients are seen in the lateral direction is the stagnation line that divides fluid from the fore and aft jets, until finally

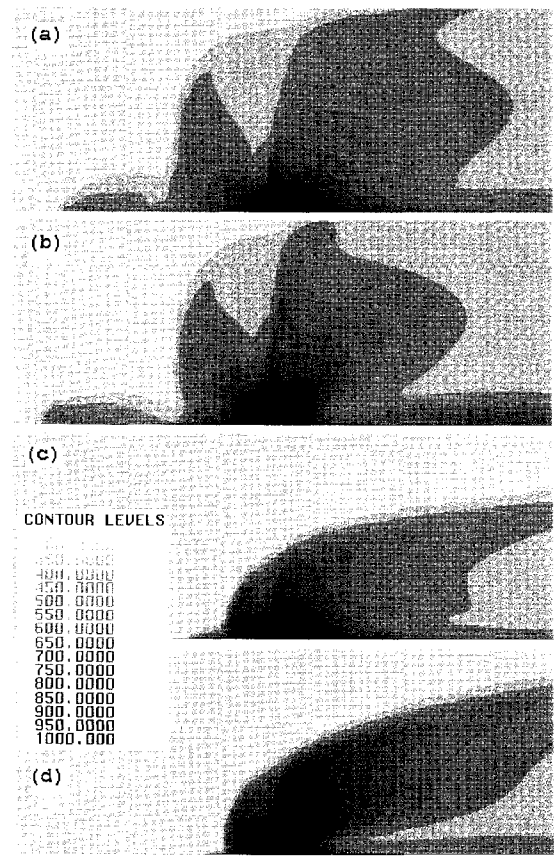

Fig. 4 Temperature contours in x-z ground plane: a) case 1; b) case 2; c) case 3; d) case 4; headwind from left to right.

Table 2 Extent of recirculating hot gas zone upstream of foreword lift jets

Case	Present Calculation	Experiments, Ref. 11
1	35	31
2	46	22
3	10	12
4	12.5	14

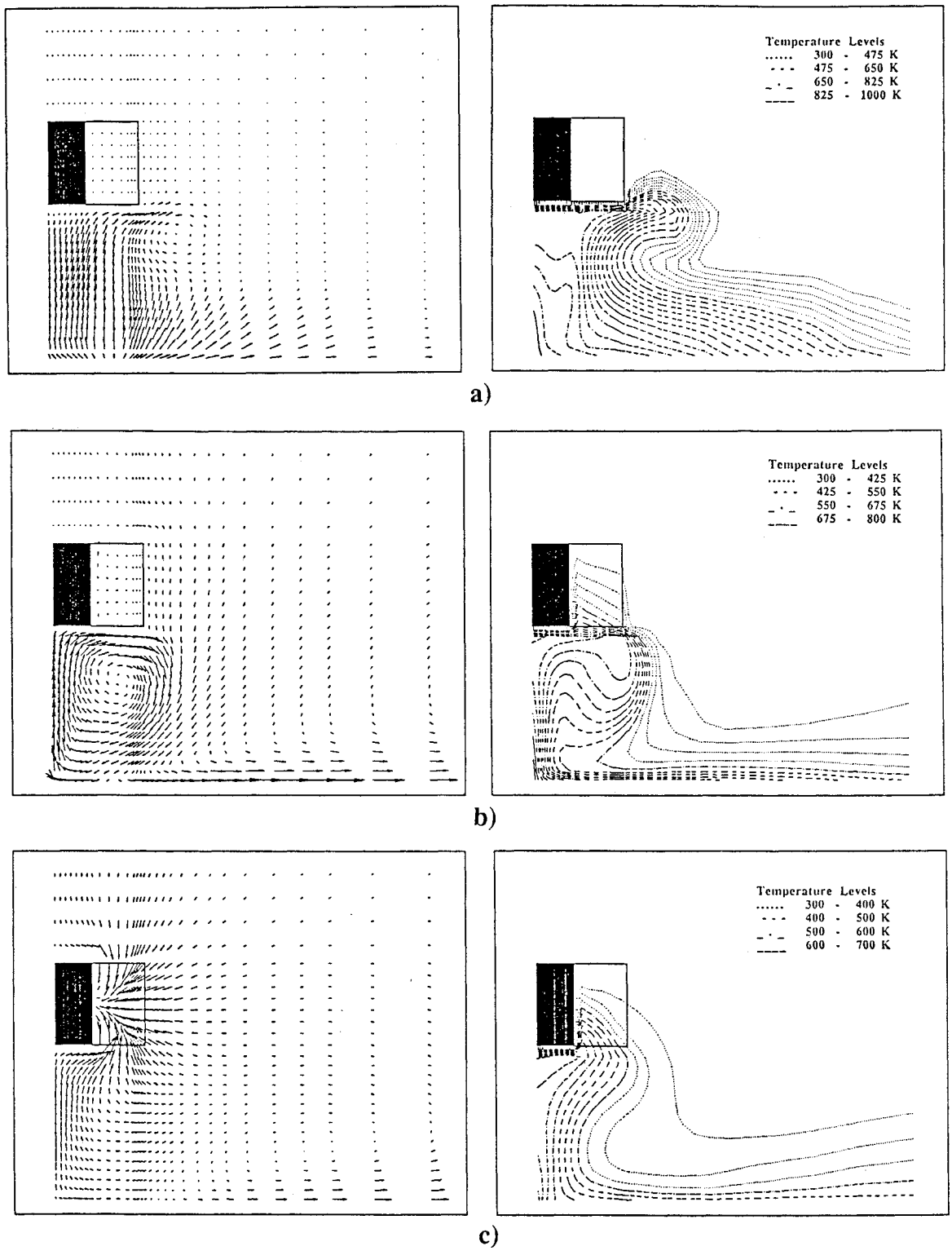

Fig. 5 Velocity vector and temperature contours in different *z-y* planes for case 1. Plot domain extends from symmetry plane to $z/d = 9$, and from ground plane to $y/d = 5$: a) $x/d = 3$; b) $x/d = -5$; c) $x/d = -10$.

they mix and smooth out the differences. These sharp gradients are also present in the simulations in Ref. 7 and in the experiments in Ref. 11, although the experimentally observed gradients are not as sharp.

Table 2 compares the upstream extent of the recirculating hot gas zone with the experiments in Ref. 11. In the present study, the temperature distribution is used as a means to determine the upstream spread of the hot gases (Fig. 3). It is seen that the calculated values agree well with the experimental values for cases 1, 3, and 4, whereas for case 2 the calculated value of x/d is much higher. Also, the trend indicated by the experiments [increased upstream penetration (x/d) with increased h/d ratio] is the opposite of what the numerical calculations indicate. This, in effect, would indicate that the jet fluid mixes more rapidly with the freestream flow and loses its identity earlier than the calculations predict. This discrepancy could be due to the inability of the k-ε turbulence model to accurately capture the full extent of turbulence production caused by the stagnating jets. Recent numerical studies of the fountain region of twin jet impingement[14] indicate that the turbulent kinetic energy is severely underpredicted, particularly in the region close to the ground plane. This, in

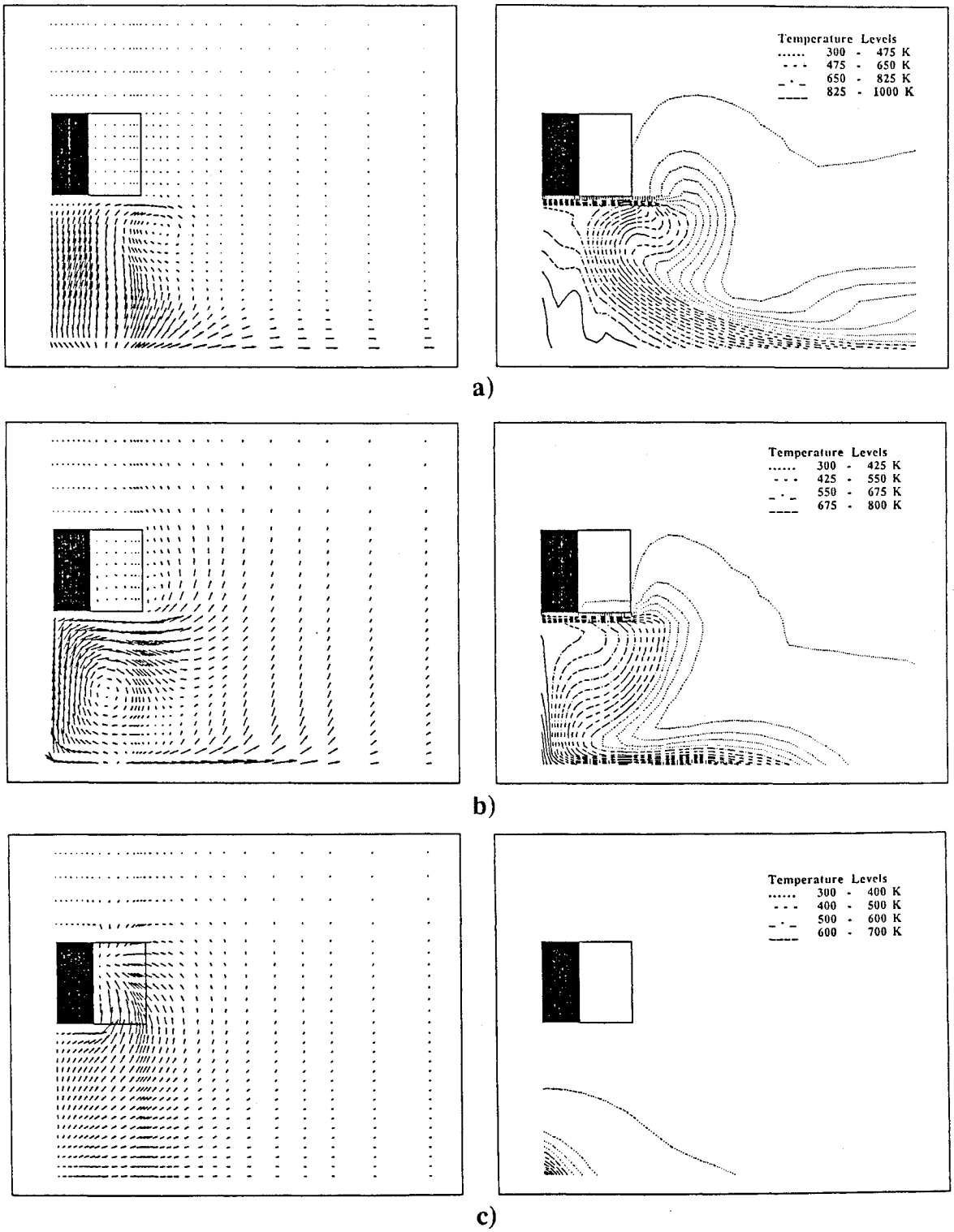

Fig. 6 Velocity vector and temperature contours in different *z-y* planes for case 3. Plot domain extends from symmetry plane to $z/d = 9$, and from ground plane to $y/d = 5$: a) $x/d = 3$; b) $x/d = -5$; c) $x/d = -10$.

part, also explains the sharp temperature gradients seen in the upwash region of the fountain flow. The authors suspect that, for case 2, this might be a critical factor in determining the dilution and spread of the jet fluid. More comparisons between the present simulations and experiments can be found in Ref. 11.

Figures 5 and 6 show velocity and temperature distributions in three *z-y* planes for cases 1 and 3. Part a) is the *z-y* plane passing through the fountain upwash between the jets, part b), the *z-y* plane between the fore jet and the inlet, and part c), the plane at the inlet. In both cases, the spanwise fountain flow responsible for the movement of hot gases upstream from the fore jets is clearly visible in b). As the hot gases from the jets move upstream under the fuselage, they are considerably diluted, due to mixing with the cooler headwind. As this gas approaches the inlet, part of it is directly ingested into the inlet c). It is interesting to see that, for the low-velocity ratio, ingestion occurs from the side, top, and bottom of the fuselage, whereas, for the higher headwind, most of the ingestion occurs from the bottom and side of the fuselage. Another interesting feature is the movement of hot gases: for the higher headwind, the hot gases show a lateral outward and upward

Table 3 Nondimensional mass averaged inlet plane temperatures $(T_{avg} - T_\infty)/(T_j - T_\infty)$

Case	Present Calculation	Calculation, Ref. 7
1	0.083	0.13
2	0.097	0.11
3	0.0	0.08
4	0.017	0.03

movement whereas for the lower headwind the flow is laterally inward, i.e., cooler fluid is entrained into the fountain region. This phenomenon is also reflected in the ground plane temperatures (Fig. 4), where the lateral spread of the jet fluid between the fore jet and the inlet is greater with the higher headwind. This is due to the higher dynamic pressure of the oncoming freestream, which forces the hot gases out from under the fuselage. Table 3 shows the mass averaged nondimensional inlet plane temperatures calculated for the four cases, and compares them to those obtained by the numerical simulations in Ref. 7. There is some discrepancy between the two calculations. It is not possible to identify the reasons for this discrepancy, but the difference in the resolution of the flowfield between the two methods could be one of the major contributing factors. The results of the present calculation follow the trends indicated by the velocity and the temperature profiles. The maximum average inlet temperature is for case 2 ($U_\infty/U_j = 0.03$, h/d = 2); case 3 does not seem to ingest any hot gases.

Summary and Conclusions

In the present paper, a multigrid calculation procedure for three-dimensional flows is used to study the hot gas ingestion by STOVL aircraft. Calculations with a simulated fuselage and twin exhaust jets have been made for two ground positions and two head-wind ratios. The global features of the flowfield (e.g., the ground plane temperature distributions and the formation of the ground vortex) for the four cases are according to expectations and agree well with the recent numerical study of Ref. 7. A major contribution of the present study is the demonstration that the multigrid algorithm can significantly reduce the computational effort required to solve the governing equations, compared to a conventional single grid procedure. The reduction in computational effort permits more parametric studies to be conducted.

In the present study, the Reynolds-averaged flow equations have been solved in conjunction with the k-ε turbulence model. The flow is considered to be steady in time, although, it has been observed[11] that the region of jet impingement is highly unsteady and the turbulence structures are very complex. Therefore, the accuracy of the current calculations is limited by the assumptions made in deriving the governing equations of the turbulence model. A study performed on the twin jet impingement flow in isolation[14] showed that the k-ε model is able to predict the velocity field reasonably well, but the turbulence kinetic energies are severely underpredicted. Although it is possible to incorporate more complex turbulence models into the current algorithm, it is not certain at this time that they improve the predictions over those of the k-ε model. Future extension of this study will be in the direction of representing the aircraft geometry more realistically through the use of curvilinear grids.

Acknowledgments

The present work was supported by Grant NAG-3-1026 from the NASA Lewis Research Center, Cleveland, Ohio. The authors wish to thank J. D. Holdeman for his encouragement during this study. The calculations were performed on the NASA Ames NAS computer facility.

References

[1]Kuhn, R. E., "Design Concepts for Minimizing Hot Gas Ingestion in V/STOL Aircraft," *Journal of Aircraft*, Vol. 19, No. 10, 1982, pp. 845–850.

[2]Kuhn, R. E., and Eshelman, J., "Ground Effects on V/STOL and STOL Aircraft—A Survey," AIAA-85-4033, AIAA/AHS/ASEE Aircraft Design Systems and Operations Meeting, Colorado Springs, CO, Oct. 1985.

[3]Agarwal, R. K., "Recent Advances in Prediction Methods for Jet-Induced Effects on V/STOL Aircraft," *International Symposium on Recent Advances in Aerodynamics*, Stanford Univ., Stanford, CA, Edited by A. Krothapalli and C. A. Smith, Springer-Verlag, New York, August 1983, pp. 471–521.

[4]Saripalli, K. R., "Lase-Doppler Velocimeter Measurements in 3-D Impinging Twin-Jet Fountain Flows," *Turbulent Shear Flows*, Vol. 5, Springer Verlag, New York, 1987, pp. 146–148.

[5]Kotansky, D. R., and Bower, W. W., "A Basic Study of the VTOL Ground Effect Problem for Planar Flow," *Journal of Aircraft*, Vol. 15, No. 4, 1978, pp. 214–220.

[6]Agarwal, R. K., and Bower, W. W., "Navier-Stokes Computation of Turbulent Compressible Two-Dimensional Impinging Jet Flowfields," *AIAA Journal*, Vol. 20, No. 5, May 1982, pp. 577–584.

[7]VanOverbeke, T. J., and Holdeman, J. D., "Three-Dimensional Turbulent Flow Code Calculations of Hot Gas Injection," *Journal of Aircraft*, Vol. 27, No. 7, July 1990, pp. 577–582.

[8]Syed, S. A., and James, R. H., "User Manual for 3D-Teach With Rotation," NASA-CR-180886, 1980.

[9]Vanka, S. P., "A Calculation Procedure for Three-Dimensional Recirculating Flows," *Computer Methods in Applied Mechanics and Engineering*, Vol. 55, 1986, pp. 321.

[10]Brandt, A., "Multi-Level Adaptive Solutions to Boundary-Value Problems," *Mathematics of Computations*, Vol. 31, 1977, pp. 333–390.

[11]McLean, R., Sullivan, J., and Murthy, S., "Hot Gas Environment Around STOVL Aircraft in Ground Proximity, Part 2: Experimental Study," AIAA 90-2269, 26th AIAA/SAE/ASME/ASEE Joint Propulsion Conference, Orlando, FL, July 1990.

[12]Launder, B. E., and Spalding, D. B., "The Numerical Computation of Turbulent Flows," *Computer Methods in Applied Mechanics and Engineering*, Vol. 3, 1974, pp. 269–289.

[13]Claus, R. W., and Vanka, S. P., "Multigrid Calculations of a Jet in Crossflow," AIAA-90-0444, 28th Aerospace Sciences Meeting, Reno, NV, Jan. 1990, *Journal of Propulsion and Power* (to be published).

[14]Pegues, W. P., and Vanka, S. P., "Numerical Study of Twin-Jet Impingement Upwash Flow," Fluids Engineering Division, Vol. 94, ASME Forum on Turbulent Flows, Toronto, Canada, June 1990, pp. 97–103.